

# Gear Diagnostics – Fault Type Characteristics

Alexander Bliznyuk<sup>1</sup>, Ido Dadon<sup>2</sup>, Renata Klein<sup>3</sup> and Jacob Bortman<sup>4</sup>

<sup>1,2,4</sup> *Laboratory for Health, Department of Mechanical Engineering, Ben-Gurion University of the Negev, Beer-Sheva, Israel*  
*bliznyuk@post.bgu.ac.il*

<sup>3</sup> *R.K. Diagnostics, Gilon, Israel*  
*Renata.Klein@RKDiagnosics.co.il*

## ABSTRACT

To date, the majority of existing Condition Indicators for gears are based on various statistical moments of a recorded time history. A supplementary analysis proposed in this study, shall suggest an approach that may, in the future, enable the identification of faulty gearwheel and possibly fault type in the system. In this work, a combined analytical and empiric approach is applied. This approach is based on the assumption that reliable dynamic models can be utilized to predict the effects of faults on vibrational patterns. Dynamic model generated signatures are used to verify experimental findings. Moreover, discrepancies between simulated and actual results, combined with understanding of the assumptions and omissions of the model, are helpful in understanding and explaining the experimental results.

A spur gear transmission setup was used for experiments, along with an electric AC motor and a friction belt loading device. The experimental runs were conducted at varying speed settings. Two types of faults, a tooth face fault and a tooth root fault, were seeded in the experimental transmission and into the model. The effect on extracted signal features is examined.

The purpose of this study is to evaluate fault detection capabilities of proposed diagnostic tools at the presence of two seeded faults of varying severity, verified by a dynamic model. Observed differences between examined fault types and their manifestation will be discussed. A basis for future work on prognostics capabilities is laid by a varying degree of tooth root fault.

## 1. INTRODUCTION

Most existing Condition Indicators (CI) for gears are defined by a statistical analysis of various signals in time or cycle domains (Dempsey, Lewicky and Le, 2007; Lewicky, Dempsey and Heath, 2010). Most of these CI are various

modifications of statistical moments (RMS, Kurtosis etc.). When applied to a gear pair time or cycle history, statistical CI differentiate between signals originating in undamaged and damaged gear pairs, but a difficulty in distinguishing between types of faults and fault location exists. In this work, an analysis of side bands of gear meshing frequencies is suggested as a tool for evaluation of gear health. Side bands analysis was proposed in other works as a tool for fault identification, and classification of side band groups was defined by Klein (2012).

This work aims to show that a more detailed analysis of faults in gears can be harvested in the order domain. In this work a concept of a division of a fault effect into two aspects, ‘dynamic’ and ‘structural’, is introduced as a possible explanation of several observed differences between faults.

Simulated vibration signals from a dynamic model, developed in the BGU HUMS lab, are compared with experimental results to help further understand the latter. Currently, the model is qualitative and purely dynamic, which means it does not account for the transmission path of the signal from its origin to the sensor.

## 2. EXPERIMENTAL SETUP

### 2.1. Setup

A simple one stage spur gear system was used in this research (figure 1). The main advantage of such a setup over a real life complex transmission lies in easier interpretation of results, for better understanding of the basic physics of this problem.

Standard (evolvent) profile spur gear pair, of module 2.5 [mm] was used, 17T driving gear (pinion) and 49T driven gear. The pinion is seated on the “In” shaft. The transmission reduces the speed of the “Out” shaft containing the driven gear and the loading device. Both shafts are supported by two ball bearings each.

Alexander Bliznyuk et al. This is an open-access article distributed under the terms of the Creative Commons Attribution 3.0 United States License, which permits unrestricted use, distribution, and reproduction in any medium, provided the original author and source are credited.

The experimental setup is driven by a 3 phase asynchronous AC induction motor. An open loop controller is used to set the frequency input of the motor. An optical encoder (24 band/revolution) is used to record “In” shaft RPS during the run.

The setup is torque-loaded via a friction belt-wheel pair. The belt is tensioned by a selectable amount of weights. The resulting side effect of bending of the shorter “Out” shaft due to radial stress is negligible.

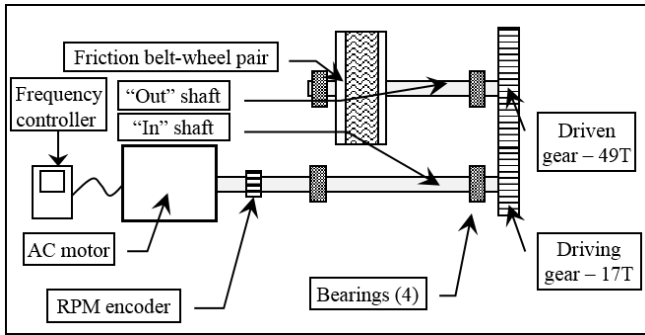


Figure 1. Experimental setup (schematic).

A Dytran tri-axial accelerometer was used to measure the vibration in the proximity of the gear mesh point. The accelerometer was fixed below the pinion, with the X axis aligned as the tangent direction at the gear mesh point, Y as the radial direction and Z as the axial direction (see figure 2).

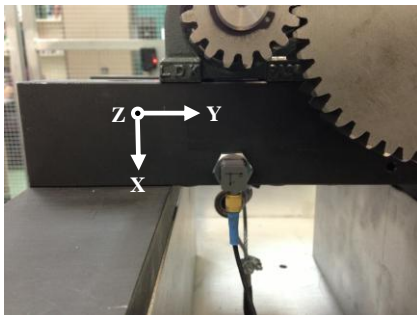


Figure 2. Accelerometer location and orientation.

### 2.2. Experiment Conduct

Experiments were conducted for each of six configurations: undamaged transmission (“Healthy”), a gear carrying a tooth face fault (“spall”), cracked pinion (“PI”), and three degrees of cracked gear (“GI”, “GII”, “GIII”). For each configuration, 20 experimental runs were performed, at four varying loadings of the friction belt and at five AC motor input frequency settings.

### 2.3. Seeded Faults and Seeding Methods

Two faults were selected for seeding in the study. The faults selected simulate common and essentially different real life faults, relatively simple to simulate both in the experimental

and model environments. A tooth face defect was seeded in the gear, simulating a fault of the spall/pitting type. The single tooth defect (figure 3) was seeded by a removal of material from the tooth face at a portion of the tooth’s width. In similarity to the effect of a common spallation (or pitting) on tooth meshing, the presence of the fault reduces the contact stiffness of the tooth, but does not yet alter the general evolute profile of the tooth.

A crack was seeded in the root of a single tooth, simulating a fatigue crack. The fault was seeded by EDM (Electro Discharge Machining) at three fault severity degrees (crack depth of 1.4, 2.1 and 3.5 mm of total tooth width of 4.8 mm) in the gear (figure 4) and at the first degree only in the pinion.

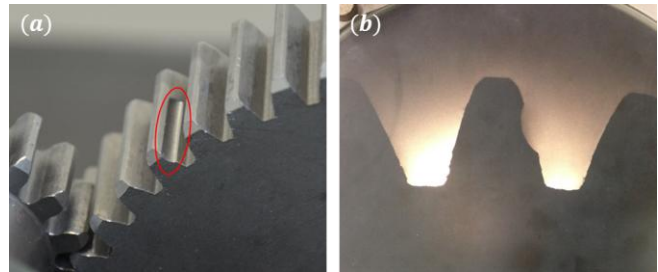


Figure 3. Seeded spalling defect (a) encircled; (b) view of the damaged tooth.

In this work, a tooth flaw is considered to have a dual effect on vibration signature. The “dynamic” component of the flaw affects the gear meshing at the point of defect, altering the dynamics behind the generated acceleration signal. The “structural” flaw alters the transmission path from the acceleration origin (gear mesh point) to the sensor.

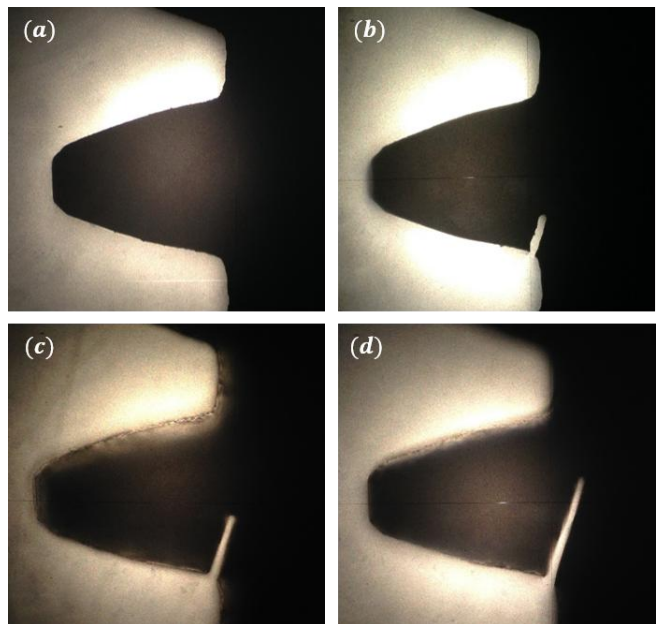


Figure 4. Seeded tooth root crack (a) healthy; (b) 1.4 mm; (c) 2.1 mm; (d) 3.5 mm.

### 3. DATA ANALYSIS

Experimentally obtained signals were analyzed in the workflow depicted in figure 5. The raw signal was resampled into the cycle domain, and then synchronously averaged. The resulting signal was then mapped into the order domain, and features were extracted from the PSD (Power Spectrum Density).

#### 3.1. Angular Resampling

As for all realistic revolving machinery, speed (RPS) was only approximately constant during the experimental runs, with relatively slight deviations from a mean value. The resulting signal is classified as non-stationary, and has “smeared” spectral contents due to the non-constant frequency of the signal periodic components. To allow for an accurate representation in the order domain, angular resampling was applied to the signal’s time history.

During angular resampling, the signal is resampled by constant rotation angle (cycle) increments rather than constant time increments as recorded originally. Signals that undergo angular resampling are said to be transferred from the ‘time’ domain to the ‘cycle’ domain. Simulated signatures (results of the dynamic model) are by definition of absolutely constant input RPS (classified as deterministic periodic signal), and therefore do not undergo this part of the processing.

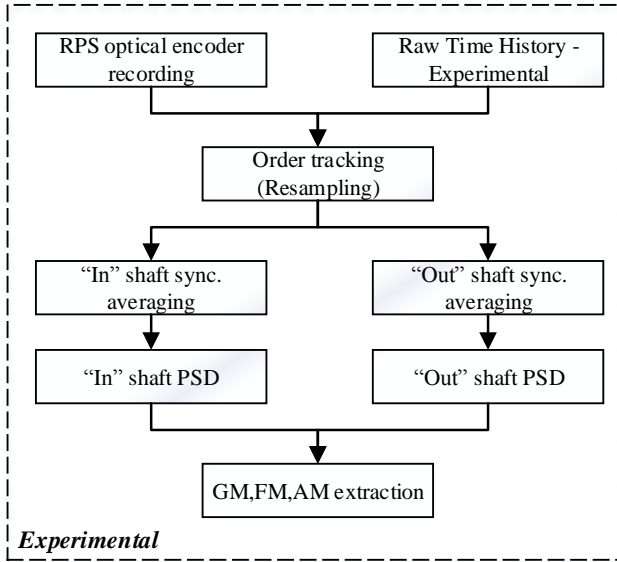


Figure 5. Experimental data analysis workflow.

#### 3.2. Time Synchronous Averaging (TSA)

The recorded data contains a substantial amount of data unrelated to the process of gear meshing. The purpose of synchronous averaging is the removal of all signal components asynchronous with the phenomena examined,

such as bearing tones, noise etc. Two TSA were calculated for each signal, by the “In” and by the “Out” shaft speeds.

#### 3.3. Calculation Error

RPS (Revolution per Second) measurement and decoding accuracy is a major error factor of calculated synchronous average and consequent PSD features. Inaccurate RPS causes smearing of PSD peaks due to averaging out of synchronous data, through inaccurate angular resampling. Although helpful with removal of noise and asynchronous components, a large amount of averaged cycles increases this error. To minimize differences between signatures, the length of measured data was set to be a constant amount of machine cycles (200) rather than a constant time interval.

#### 3.4. Order Feature Extraction

The synchronously averaged signals were mapped from the cycle domain to the order domain by a windowed Welch’s periodogram. From the PSD (Power Spectral Density), three features were calculated.

The gear mesh order is the  $z^{\text{th}}$  shaft harmonic (where  $z$  is number of teeth on shaft’s gearwheel). The sum of the first five harmonics of gear mesh amplitude in the PSD was defined as the GM feature. The GM is assumed to carry the energy resulting from the meshing of all (defective and healthy) teeth. The GM is identical whether it is calculated from the “In” or the “Out” shaft synchronous average.

$$GM \equiv \sum_{h=1}^5 \hat{x}(h \cdot z \cdot f_s) \cdot df \quad (1)$$

As described in other publications (Klein, 2012), sidebands (SB) in the order domain on both sides of the main gear mesh frequency are caused by the amplitude and frequency modulations of the shaft speeds. These take the form of accompanying pairs of peaks, at constant spaces (equal to the modulating wave frequency), as can be seen in the example in figure 6. Two types of sidebands were observed in all signatures – those associated with the “In” shaft and those associated with the “Out” shaft.

Sidebands groups that were considered in this study as features are:

- AM (Amplitude Modulation) – the sum of amplitudes of the first two (as defined by Klein in 2012) pairs ( $n=1$  to 2) of SB around a GM harmonic:

$$AM \equiv \sum_{h=1}^5 \sum_{n=1}^2 \hat{x}((h \cdot z \pm n) \cdot f_s) \cdot df \quad (2)$$

- FM (Frequency Modulation) – sum of all the other available SB amplitudes that can be associated with the GM harmonic. The association limit in the order domain was set to be mid-way between adjacent GM harmonics ( $n=3$  to  $z/2$ ):

$$FM \equiv \sum_{h=1}^5 \sum_{n=3}^{z/2} \hat{x}((h \cdot z \pm n) \cdot f_s) \cdot df \quad (3)$$

Each feature (FM, AM) was calculated by the summation of all related peak amplitudes for the first five harmonics (denoted h) of GM.

Individual peaks in the spectrum are associated with dynamic effects that originate from the machine rotation. Therefore they occur at discrete frequencies, which are multiplications of the machine rotation speed. Transmission path is composed of structural effects that are not dependent on rotation. Transmission attenuates or amplifies the dynamic peaks and all other frequencies, and is continuous. The curve in the spectrum (Klein, 2013) which represents the transmission path is illustrated in figure 7.

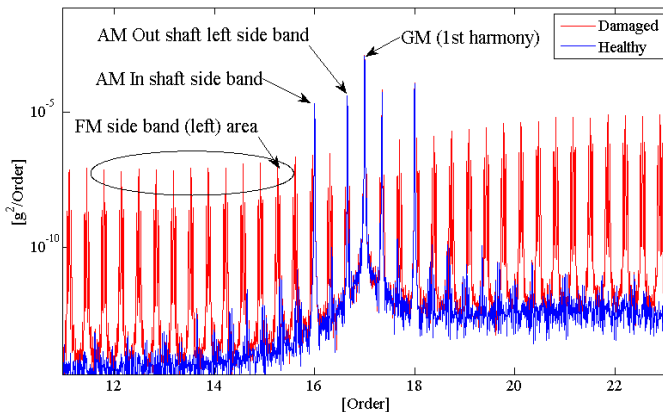


Figure 6. Example of GM, FM, and AM manifestation in PSD of a pair of simulated runs (with/without flaw). In example shown, seeded fault can be observed in “Out” shaft FM sideband increase.

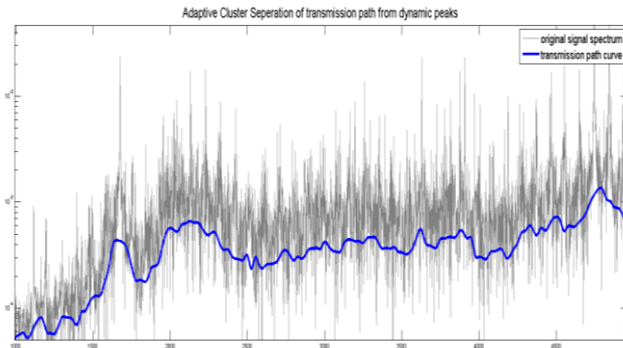


Figure 7. Example of the manifestation of dynamic reciprocating effects as peaks (grey) over a general transmission path spectral curve (blue)

### 3.5. Cycle Domain Analysis

RMS and kurtosis were calculated for both synchronously averaged cycle domain (resampled) signals (by In and Out shafts). These were calculated both for the complete signal and for the residual (as defined by Dempsey et al, 2007).

These moments are currently the basis for most common Condition Indicators for gears.

### 3.6. Spherical Coordinates

It is assumed that the transmission function alters both the magnitude and direction of the generated vibration. A spherical coordinates approach is proposed in this study (equation 4). Among the advantages of this approach is the measurement of fault effect on vibration magnitude, rather than one dimensional vibration changes which are an incomplete representation of the fault manifestation.

Spherical magnitudes were calculated from the tri-axial signal (equation 4).

$$\|\bar{a}\| \equiv \sqrt{a_x^2 + a_y^2 + a_z^2}, \quad \bar{a} \in R^3 \quad (4)$$

The same data analysis that was performed for the recorded separate axis was repeated for the vector magnitude of the spherical coordinates.

Spherical magnitudes analysis allows the consideration of vibration magnitude only, detached from vibration direction.

## 4. DYNAMIC MODEL

Following the procedure described in our previous article (Dadon et al 2014), a qualitative dynamic model of a spur gear transmission is developed in order to describe the dynamic vibration response of the experimental gearbox system. The following description of the model is concise, since the modeling is not the primary subject of this article.

The experiment system (figure 1) was idealized and all of its components were incorporated in the dynamic model, as shown in the scheme in figure 8. A constant input velocity and external applied load are the boundary conditions, which are chosen to simulate the experimental settings.

The interaction of a gear pair is modelled by linear springs with a varying mesh stiffness, which is dependent on the angular position of the gears. The stiffness of a spur gear tooth is determined by considering the strain energy, Hertzian contact and gear body-induced tooth deflection due to contact of teeth (Chaari, Baccar, Abbes and Haddar, 2008; Chen & Shao, 2011). Two directions of transverse displacements are examined, radial and tangential.

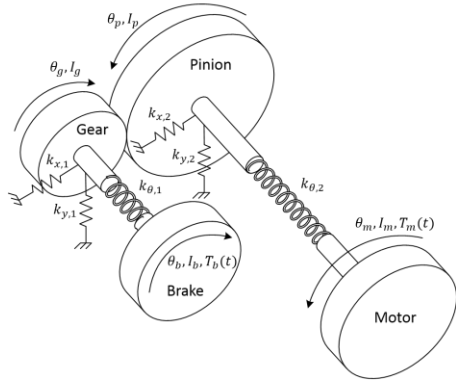


Figure 8. Spur gear system model

The coupled differential equations of the non-linear multi degree of freedom (MDF) system, describing the motion of the specified system, are derived from the Euler-Lagrange equations. The general form of the equations is therefore

$$[M]\{\ddot{u}\} + [C]\{\dot{u}\} + f_s(\{u\}) = \{F_{ex}(t)\} \quad (5)$$

Where  $u$  is the vector of generalized coordinates, given by

$$u = \{x_1, y_1, x_2, y_2, \theta_g, \theta_p, \theta_m, \theta_b\}^T \quad (6)$$

$[M]$  is a diagonal mass matrix,  $\{F_{ex}(t)\}$  is the external excitation force vector and  $f_s(\{u\})$  is a non-linear relative displacement function. The non-linearity is a result of the structural stiffness matrix, particularly the variable gear mesh stiffness. The coupled differential equations are solved using Newmark's numerical method (Chopra, 2001).

The effect of described seeded tooth faults on the dynamic response is expressed by alteration of the gear mesh stiffness. The geometric form (type, location and size) of a fault defines the gear mesh stiffness alterations as function of mesh angle. In this manner only the dynamic effects of a fault are considered. Since the transmission path effects between the signal origin and the sensor are not modelled, structural effects of a fault are not accounted for.

Results obtained via the dynamic model are titled in this paper 'simulated results'.

## 5. RESULTS

Both experimental and simulated (model) results are described in this chapter. Typical results are displayed in the following figures. It was found that available loading capability in current experimental setup is negligible when compared with the effects of varying rotation speed, therefore all charts are displayed as a function of varying RPS.

### 5.1. Statistical Moments (Cycle Domain Analysis)

Spall fault was manifested in RMS increase in both residual and ordinary TSA signals of the In shaft. The spall fault was not manifested in kurtosis.

First degree of gear crack was not detected by cycle domain analysis (RMS and kurtosis). The pinion crack was detected primarily by an increase in RMS of the Out shaft, more pronounced in the residual signal.

Second and third degree gear cracks were very similarly detected by an increase in RMS of both shaft.

To conclude, except gear crack I, all faults were detected by RMS. Kurtosis remained unchanged by all types of seeded faults.

### 5.2. Order Features

The GM feature was not found to be a good fault indicator, but was the prime reactant to load changes, in good accordance with the simulated results. The AM feature was anticipated by the simulated results to be a secondary fault indicator, but in experiments was overwhelmingly affected by shaft imbalance and gear eccentricity. This was also verified by simulated runs with increased imbalance. FM seems to be the primary feature for consideration.

### 5.3. Fault Detection

Two types of seeded faults were studied, as described in chapter 2. The spall fault was seeded in the gear. A tooth root crack was seeded in both the gear and the pinion (separate experiments). It was observed that all faults were detected primarily in the FM feature.

As can be observed in figure 9, all seeded faults (gear spall, gear crack, pinion crack) cause a significant change in FM (In, Out or both). The most noticeable fault proved to be a pinion tooth root crack, with a significant increase of FM Out (Tangential).

Spall fault caused an increase of In shaft FM. A minor increase of FM Out was observed.

Generally, all fault manifestation increased with growing RPS. The dominant axis for fault manifestation was the tangential, thus chosen for display in all figures.

In simulated results, similar curves of FM increase vs. RPS were calculated. Simulated FM of shaft not carrying the faulty gearwheel (e.g., Out for PI) exhibited the same behavior but at substantially lower amplitudes (thus indiscernible in figure 10).

### 5.4. Fault Type Diagnosis

As can also be seen in figure 9, a variety in FM response to seeded flaw exists. For example, substantial increase in FM

Out is associated with crack (pinion or gear) and not with spall.

A more significant difference between crack and spall faults is in the overall spectrum curve, representing the structure effects. The spall fault has a minor structural manifestation, and is mostly a dynamic fault, whereas cracks have a significant structural effect on the vibration signal travelling from the origin to the sensor. Therefore crack faults alter the transmission path more than spall faults. This alteration of the transmission path (and as a result, the overall spectrum curve) may offer a tool to differentiate between the two fault types.

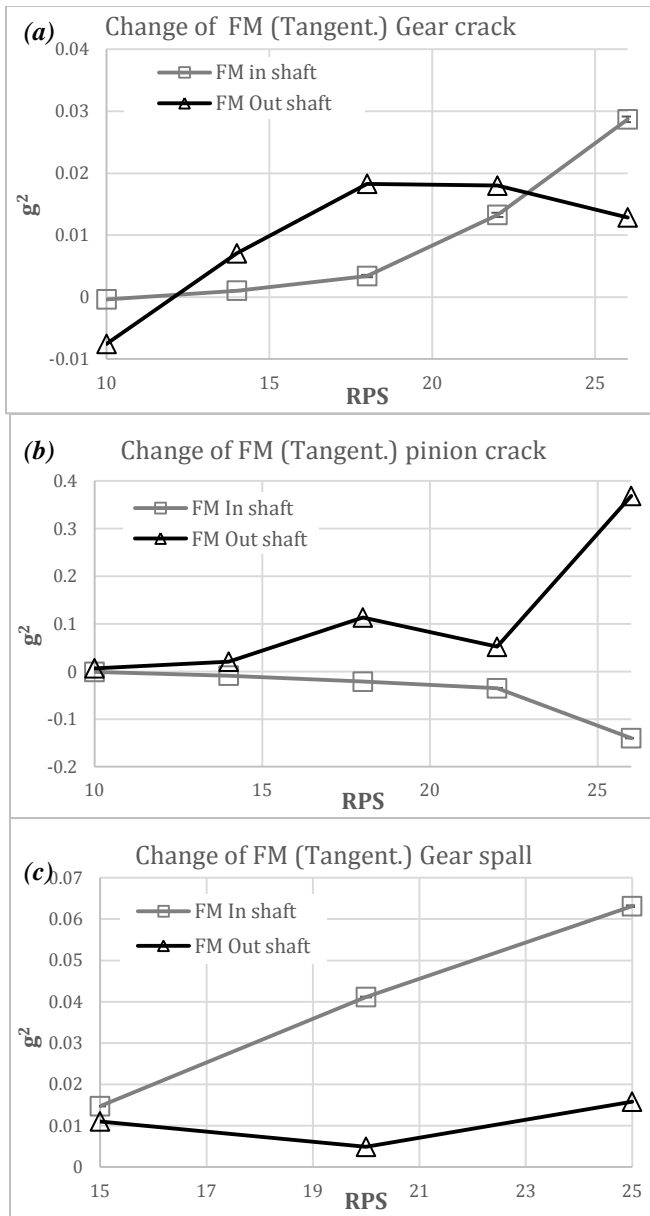


Figure 9. Increase or decrease of Experimental FM Tangential (In & Out) as a result of, (a) gear crack, (b) pinion crack, (c) gear spall

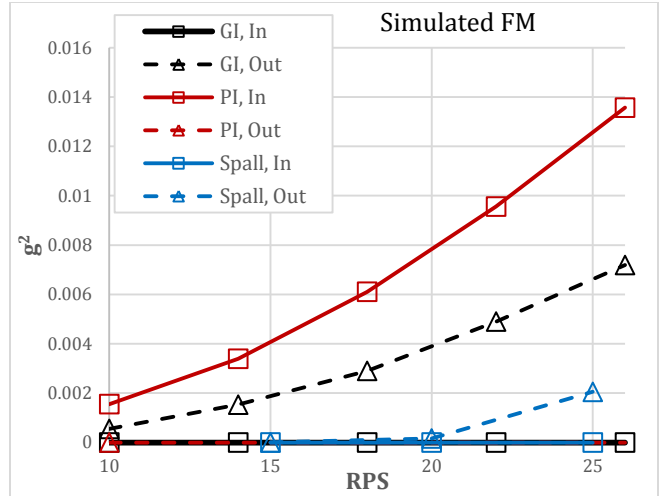


Figure 10. Increase of Simulated FM (In & Out) as a result of Spall, gear crack and pinion crack.

In figure 11(a), a damaged (spall) and healthy frequency domain PSD of similar RPS and load conditions are shown (tangential axis). The underlying transmission function curves of the healthy and damaged signatures are similar, and the main differences are in the side bands amplitudes of the 1<sup>st</sup>, 2<sup>nd</sup> and 3<sup>rd</sup> harmonics of the gearmesh frequencies. In comparison, in figure 11(b) four runs (healthy, GI, GII, GIII) are shown. In this case, the transmission functions vary significantly, with major differences arising above 850 Hz. Since the only difference between the runs is the severity of the crack, the fault effect on transmission function (expressed by overall spectrum curvature) is hereby shown.

### 5.5. Identification of Faulty Machine Gear Wheel

In this work, identification of faulty machine gear wheel is not achieved. Nevertheless, a suggestion arises as to a possible research direction for identification of fault location.

Crack location (gear/pinion) may be deduced from the effects of the structural aspect of the fault. As already discussed, FM related to shaft carrying the faulty wheel is attenuated in comparison with FM of shaft not carrying the faulty wheel. As can also be seen in figure 9, for higher RPS (22,26) FM related to faulty shaft is expressed in downward sloping (concave) curve, while the healthy shaft's FM has an upward sloping (convex) curve response. While the latter fits curvature predicted by simulations for all faults at all locations, the former does not.

FM feature is extracted at specific (constant) locations in the order domain, while the system transmission function is constant in the frequency domain. Changing RPS causes a shift of the order domain in relation to the frequency domain. Ergo, curves of FM as function of RPS depend on transmission function. A change in these curves due to

introduction of a fault suggests an alteration of transmission function by the seeded (structural) fault.

Signals that travel from the mesh point (vibration origin) through the healthy gearwheel are unaffected by the crack, while signals travelling through the cracked gearwheel experience a modified transmission path due to the crack. This suggests that FM In is not affected by the structural element of the crack, while FM Out is.

The nature of FM curve as a function of RPS is a property of initial (healthy) transmission and machine in question, and is therefore a case specific phenomenon. It may be possible to differ between gear and pinion cracks in this manner in the future, but further study and modeling of the transmission function is required to generalize and verify this special case observation.

**5.6. Fault Severity**

The fault is seeded in the gear, seated on the Out shaft. As can be seen in figure 12(a), a gradual increase in FM In side bands is obvious as tooth root crack propagates, making it possible to assess fault severity levels. All curves exhibit similar RPS dependency of a rising slope (concave). FM In dependence on RPS fits simulated results for FM Out (figures 12, 13).

- FM Out response to fault severity is a notable increase from healthy to GI, an additional increase to GII, and an unexpected drop in values for the maximal severity GIII.
- FM Out (RPS) curves are of a different (convex) nature, especially for GIII.

Both these properties of the FM Out were not anticipated by

the simulated results and are not observed in FM In. As explained in chapter 5.5, this may be reasoned by the structural effect of the fault on the transmission function.

In cycle domain analysis, residual signals are dominated entirely by the FM feature (with GM and AM removed). As to be expected, very similar figures regarding crack severity were achieved by a calculation of the RMS of the residual of synchronously averaged signals (by In and Out shafts).

Simulated FM In response to crack on the Out shaft gear was very similar to simulated FM Out (shown in figure 13), at lower amplitudes.

**6. DISCUSSION**

**6.1. Order Domain Analysis Capabilities**

In all acquired results, the FM feature was the most reliable indicator of the presence of a seeded fault. All faults were readily discernible in a change of FM. Varying load had a less significant effect on FM increase, perhaps due to limited loading capability of available apparatus. It was shown that higher RPS produces significantly better fault expression in FM, in accordance with simulated results.

Distinguishing between different faults and fault location may be accomplished in the future by observations in the order domain as depicted in chapter 5. This requires further study of the transmission function alteration by the seeded fault ('structural' aspect of the fault), and additional study cases before any definitive conclusions can be made.

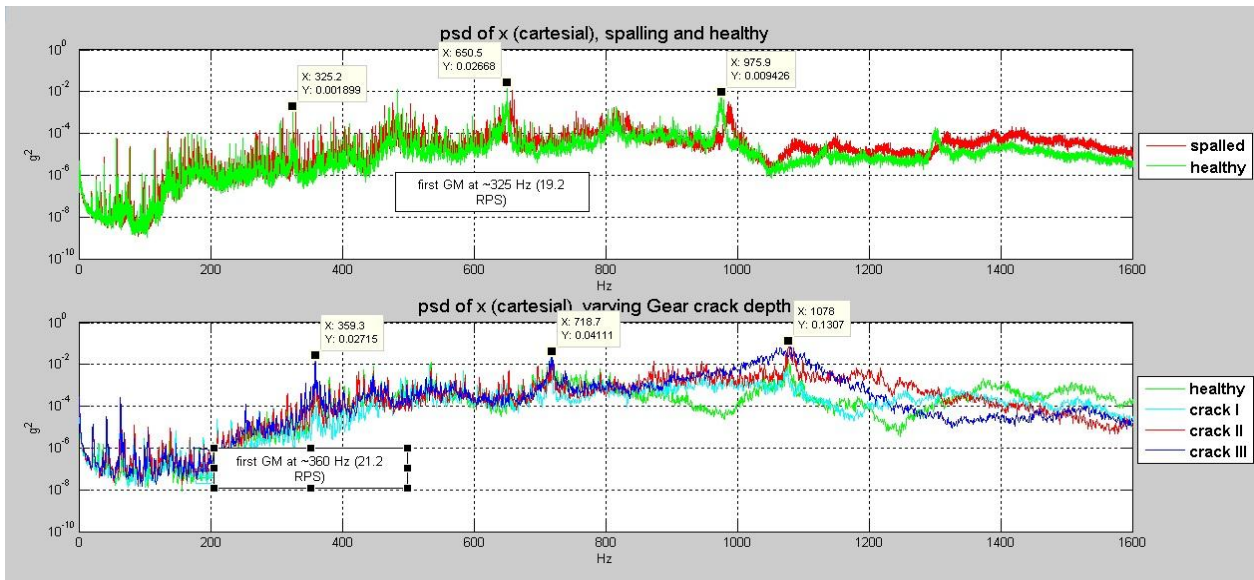


Figure 11. PSD (tangential) of frequency domain, (a) spall vs. healthy, (b) various degrees of cracked gear

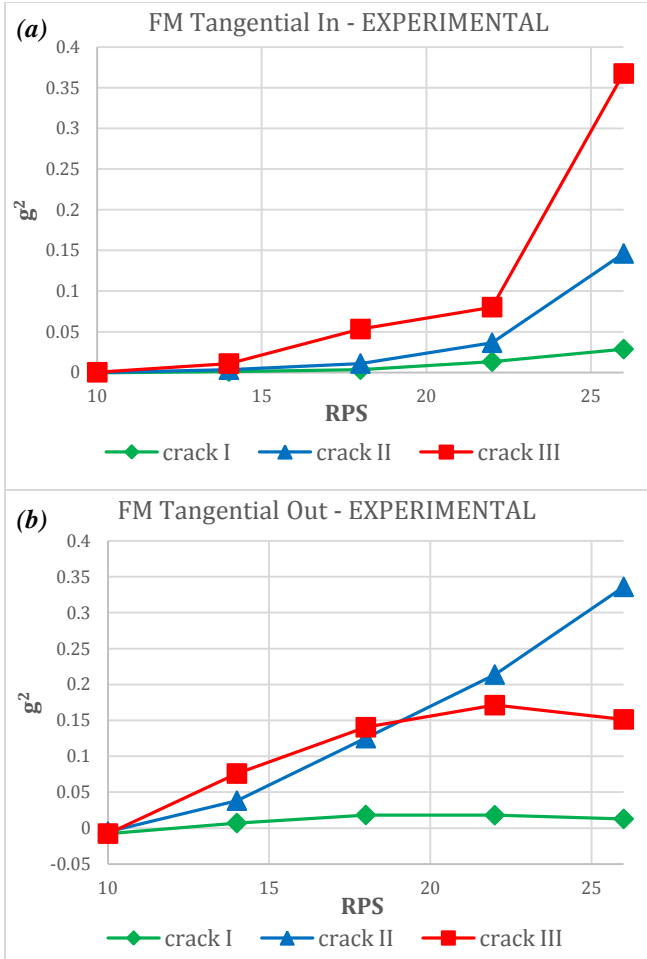


Figure 12. Increase of FM Tangential (a) In (b) Out at three levels of crack (gear).

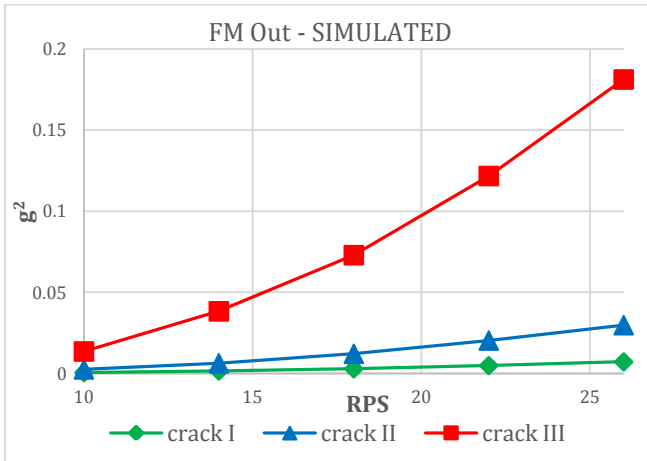


Figure 13. Increase of FM Out at three levels of crack – Simulated results.

A growing severity of a gear tooth root crack was manifested in FM In (not fault carrying shaft), with values of side band increasing in an obvious correlation to crack

size. The fault carrier shaft (Out) showed an unexpected drop of FM for crack III (figure 12(b)).

### 6.2. Simulated results comparison

Two discrepancies are observed in the simulated versus experimental results.

FM of shaft not carrying the fault is almost idle in the simulated results. In the actual measurements FM of both shafts was affected by the fault. Crack deepening causes a similar response in FM Out (figure 13) as observed in the other shaft in experimental results (figure 12(a)). A coupled response of both shafts to all faults is observed in experiments. This coupling is much weaker in the dynamic model equations.

Current version of the dynamic model does not account for the effects of transmission function on the dynamic response of gear meshing. Furthermore, the alteration of transmission function caused by faults is not included in the model. In regards to the distinction between dynamic and structural faults, the model currently deals with the ‘dynamic’ component only. It is likely that most of the discrepancies between simulated and actual results are explained by this deficiency.

### 6.3. Spherical vs. Cartesian Coordinates

Most of the extracted features and trends discussed were visible in the Cartesian (tangent, radial, axial) separate axis analysis, but crack fault manifestation was not consistent: some experimental runs showed an increase in tangential, or radial axis, with no obvious pattern as to which axis responds to the fault and under which conditions. In several runs, only one or two out of the three axis responded to the fault.

Representation in spherical coordinates (vibration vector magnitude analysis) enhanced the results and improved consistency and similarity between runs, with overall magnitude FM behaving in a consistent manner over varying RPS (examples in figures 14, 15).

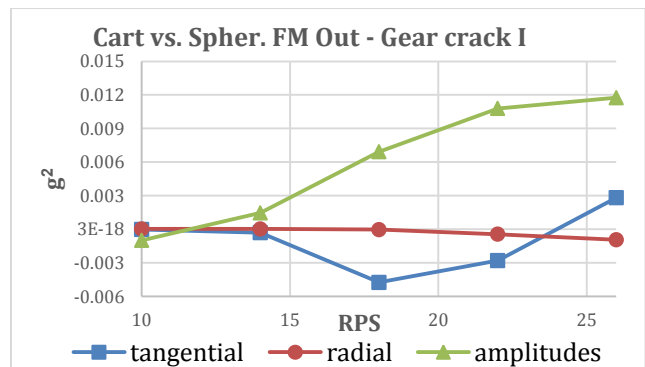


Figure 14. Spherical and Cartesian coordinates FM Out. Shown are FM Out sums related to #1 harmonic only.

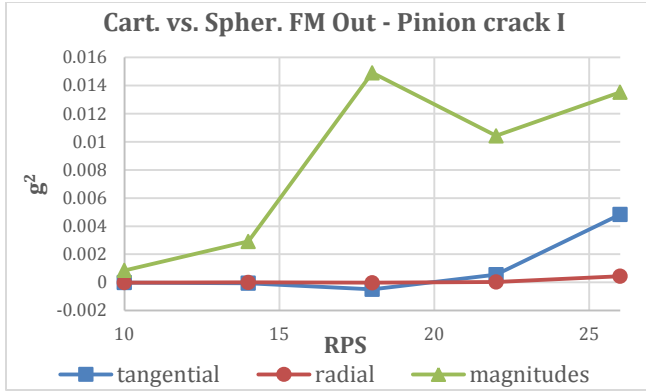


Figure 15. Spherical and Cartesian coordinates FM Out. Shown are FM Out sums related to #1 harmonic only.

In the scope of this work, only magnitudes were considered and analyzed. Some information is lost in the transition from Cartesian coordinates, specifically the effect of fault on vibration vector orientation.

A possible solution to the specified problem, and a subject of further research may be the same spectral analysis applied to an angular property of the acceleration vector.

In figure 16 the same information as in figure 11 is shown for the spherical magnitudes. It can be seen that transmission function of the magnitudes is less affected by the introduction of gear crack than the transmission function in the tangential direction only. This suggests that the alteration to the transmission function in shown bandwidth is mainly in changing the direction of the vibrating signal and not by introduction of natural frequencies (local amplifications of vibration). Attenuation of tangential signal for a certain frequency, for example low amplitudes for healthy tangential signature around 950 Hz, is compensated by high radial and/or axial amplitudes around 950 Hz, and thus spherical magnitude is unaffected. This hints to the possible importance of the analysis of acceleration (unit) vector direction oscillation.

### 7. CONCLUSION

Order domain features, and specifically FM, may be utilized as a supplementary or even a leading fault indicator. Crack size seems to be directly correlated with FM side bands energy.

The separation of fault effect on vibrations to ‘structural’ and ‘dynamic’ components was defined. The same approach may be utilized in the analysis of the signal. An extraction of the transmission path curve from the PSD may allow for a separate analysis of fault effect on transmission (‘structural’) and on features extracted from a PSD without a transmission function (‘dynamic’). The features calculated in this work were not separated in this manner, and the effects of one and the other intertwined.

A deeper understanding and analysis of the ‘structural’ effects of a flaw may lead to better discrimination between types of faults and identification of faulty gear wheel.

Current simulated results are purely ‘dynamic’, as explained in chapter 6. A Finite Discrete Element scheme or another numeric supplementary tool can be used to simulate the ‘structural’ aspect, to achieve a more complete simulated picture.

A continuous dialogue between an analytic model approach and actual experiments analysis is crucial when attempting to understand the physical nature of the problem at hand. Discrepancies between the simulated and experimental results tend to originate from assumptions made in the design of the model. This idea facilitates the identification of the origins of these features.

The advantages of proposed spherical coordinates (magnitude and direction) were exhibited. The spherical coordinates enhance results which are random in direction but consistent in overall vector magnitude. Faults that primarily alter the direction of a vibration may require the more traditional Cartesian approach, or an analysis of the directional component of the spherical coordinates.

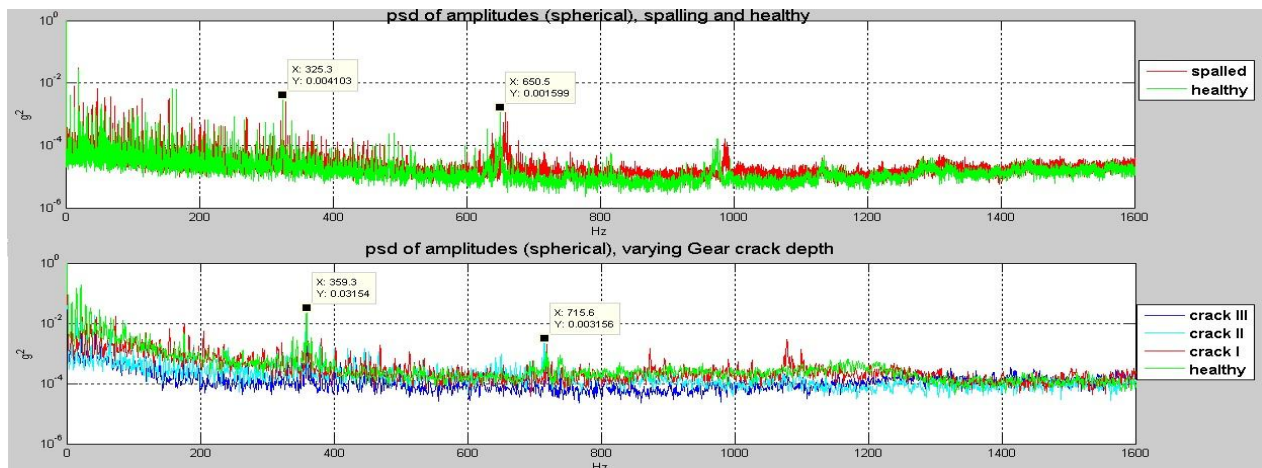


Figure 16. PSD (spherical) of frequency domain, (a) spall vs. healthy, (b) various degrees of cracked gear

**NOMENCLATURE**

$GM$	energy summation of the gear mesh feature
$h$	harmonic index
$\hat{x}$	Fourier transform of $x$
$z$	number of teeth on gearwheel
$f_s$	shaft frequency
$df$	frequency\order resolution
$AM$	energy summation of the amp. modulation feature
$n$	sideband index
$FM$	energy summation of the freq. modulation feature
$\bar{a}$	acceleration vector in the time domain
$a_x$	Tangential component of the acceleration vector
$a_y$	Radial component of the acceleration vector
$a_z$	Axial component of the acceleration vector

**REFERENCES**

- Dempsey, P. et al., (2007). Investigation of Current Methods to Identify Helicopter Gear Health. NASA, Glenn Research Center, Cleveland, Ohio, USA.
- Lewicky, D. et al., (2010). Gear Fault Detection Effectiveness as Applied to Tooth Surface Pitting Fatigue Damage, *Gear Technology Nov./Dec. 2010* pp.48-59, Randall Publications LLC
- Klein, R.,(2012). Condition Indicators for Gears. R.K. Diagnostics, *Annual Conference of Prognostics and Health Management Society 2012*, Gilon, Israel.
- Klein, R.(2013). Comparison of Methods for Separating Excitation Sources in Rotating Machinery. R.K. Diagnostics, Gilon, Israel.
- Dadon, I., Bliznyuk, A., Klein, R., & Bortman, J. (2014). Towards a reliable non-linear dynamic model of damaged gear transmission. *The Eleventh International Conference on Condition Monitoring and Machinery Failure Prevention Technologies*, June 10-12, 2014 Manchester, UK.
- Chaari, F., Baccar, W., Abbas, M. S., & Haddar, M. (2008). Effect of spalling or tooth breakage on gearmesh stiffness and dynamic response of a one-stage spur gear transmission. *European Journal of Mechanics-A/Solids*, Vol 27, pp 691-705.
- Chen, Z., & Shao, Y. (2011). Dynamic simulation of spur gear with tooth root crack propagating along tooth width and crack depth. *Engineering Failure Analysis*, Vol 18, pp 2149-2164.
- Chopra, A. K. (2001). *Dynamics of Structures*. USA: Prentice Hall.